Thermal Response Simulation of Tetralayer Thin Film Structure under Ultrafast Laser

Saffa Issam Mohamad Ali, Haidar Jawad Mohamad and Mohammed Jassim Mohammed Ali
Department of Physics, College of Science, Mustansiriyah University, 10011 Baghdad, Iraq
saffaissam@uomustansiriyah.edu.iq, haidar.mohamad@uomustansiriyah.edu.iq,
mohammedjassim@uomostansiriyah.edu.iq

Keywords: Ultrafast Laser, COMSOL Simulation, Thin Film, Thermal Effect, Four-Layer Structure, Heat Transfer, Laser-Induced Heating.

Abstract: Spin current in spintronics devices is mostly affected by the thermal gradient within storage devices. In this current study, the thermal response of a tetralayer thin film structure in a three-dimensional numerical simulation was observed. This model was exposed to irradiation by an ultrafast femtosecond pulsed laser. On nanosecond timescales, the model integrates heat transfer in solids to show both the energy absorption and subsequent thermal diffusion accurately. The tetralayer sample was composed of ferromagnetic (FePt)/ferromagnetic (Py)/spacer (Cu)/magnetic insulator (YIG) sequentially. Parameters such as thickness and time were shown to have a major effect on the generated spin current, as proven and shown by the simulation results. In addition to that, the temperature gradients within the tetralayer are crucial for generating the spin current and demonstrate the significant influence of material characteristics and layer location on the governance of ultrafast thermal transport in multilayer thin film systems. Through most of the simulation experiments, the FePt layer experiences the most significant and noticeable temperature increase after the laser excitation.

1 INTRODUCTION

Spintronics, ultrafast pulsed lasers, and heat-assisted magnetic recording (HAMR) are recognized as revolutionary inventions in modern computing and information systems [1].

Each of these subjects pushes the boundaries of data processing, storage, and manufacturing through different physical principles [2].

Spintronics uses electrons' inherent spin and their charge as a means to store and process data. Spintronics devices, compared to traditional electronics, achieve faster processing speeds, lower power consumption, and higher integration density [1], [2].

Ultrafast pulsed lasers are essential instruments in precise material processing, biomedical applications, and nonlinear optics. Ultrafast lasers are known for their suitability in applications that require little heat diffusion and localized contact because of their ability to produce brief, high-intensity energy bursts [3]. Ultrafast pulses range from femtoseconds to picoseconds. Their ultrashort duration concentrates energy in time, enabling high precision, minimal heat diffusion, and ultra-fast interactions [4], [5].

As conventional magnetic recording technologies reach their limits, HAMR emerges to resolve this problem by allowing the writing of data at much finer scales because of temporarily heating the recording medium above its Curie temperature, leading to a reduction in coercivity [6]. HAMR technique records a data on a storage medium. This method employs a laser to reduce magnetization on a femtosecond timescale to record the data [7].

Laser power generates heat in the storage sample which reduces the coercive field in an inverse proportional relationship. Therefore, the sample layers must have a high magneto-crystalline anisotropy [8].

Comprehending the thermal behavior of multilayer thin films under these irradiation circumstances is essential for the design of resilient, high-power optical components [9]. Both ferromagnetic and magnetic insulators are essential to the creation of the spin current due to their varying heat conductivity, which will produce heat along all layers in varying percentages. Multilayer thin films

used to achieve the spin current, which typically consist of ferromagnetic, ferromagnetic, spacer, magnetic insulator [4], [10].

The relationship between ultrafast laser excitation and spin transport in multilayer thin films has been the topic of extensive research over the last decades. J. Kimling *et al.* (2017) used a theoretical model to describe spin diffusion in heterostructures that consist of normal-metal and ferromagnetic-metal during pulsed laser heating, where spatial gradients drive spin diffusion currents. The findings show that the spin-dependent Seebeck effect was amplified by the spin heat accumulation, highlighting its important significance in ultrafast spin transport phenomena [11]. M. A. Abdul-Hussain *et al.* (2021) used an ultrafast femtosecond laser in a thin multilayer structure consisting of Al_2O_3/$Ni_{81}Fe_{19}$/Copper/$YFeO_{12}$/Gd_3GaO_1, at room temperature to generate the thermal gradient behavior required to obtain the spin current. Thermal behavior and temperature gradient within the trilayer system were supported by a theoretical framework and modeled using COMSOL software. The results indicated that the thickness of different layers considerably influences the spin current generation by establishing a considerable thermal gradient in the magnetic insulator [9]. H. J. Mohamad *et al.* (2025) used COMSOL software to understand the temperature behavior of the laser pulse on the suggested sample FePt (8 nm) /MgO (8 nm) /SiO2 (58 nm) /Si (9.32 E-7 m)، in which HAMR use was the focus of this study. The femtosecond pulsed laser is simulated depending on the reflected, transmitted, and absorbed laser light. The pulsed laser has a significant impact on the temperature rise in the FePt layer. The result showed that the laser power depends on the layer's thickness, which gives a high temperature gradient within the sample layers and leads to saving energy [12] .

The previous studies [18]–[20] have examined trilayer and other multilayer configurations subjected to ultrafast laser excitation. This work introduces a tetralayer FePt/$Ni_{81}Fe_{19}$/Cu/YIG structure that merges both ferromagnetic metals and a magnetic insulator to more realistically represent spintronic stacks used in next-generation HAMR devices.

The earlier simulations and studies primarily focus on single layer or trilayer systems. In contrast, the present model enables the quantitative observation of heat transport across multiple interfaces, highlighting the role of different material properties and layer ordering in determining the efficiency of spin current generation.

This represents a step forward toward optimizing multilayer geometry for ultrafast spin caloritronic applications.

In the present study, COMSOL Multiphysics (v 6.1) was used to simulate the results involving the ultrafast (fs) laser. These pulses are used to induce thermal behavior inside the nano-sized tetralayer FePt/Ni81Fe19(Py)/Cu/Y3Fe5O12(YIG) sample.

A large temperature gradient is produced within the tetralayer structure sample as a consequence of the femtosecond laser pulse, which causes the ferromagnetic overlayer to undergo partial demagnetization.

Through the use of a spacer, the electron spin is effectively transferred to the magnetic insulator. The fundamental challenge consists of recreating the ultrafast pulsed laser and analyzing the temperature difference within the tetralayer as a function of both the passage of time and the thickness of the sample.

2 THEORETICAL CONSIDERATION

Ultrafast lasers operate in the picosecond (ps) to femtosecond (fs) range, with pulse durations shorter than the electron-lattice relaxation time. As a result, the energy is initially deposited into the electron system, which then transfers heat to the lattice via electron-phonon coupling [13].

The laser spot diameter is established at 120 μm, and the entire width at half maximum of the pulse duration (t) is presumed to be 74 femtoseconds. The laser functions at a repetition rate (f) of (100) kHz. Based on these parameters, the peak power (P), expressed in milliwatts and can be found using the following expression [13] :

$$P = \frac{\text{power } (mW)}{f \times t} = \text{power}(mW) \times 1.3514 \times 10^8. \quad (1)$$

Ultrafast laser pulses, with durations on the femtosecond timescale, induce rapid temperature rises within multilayered sample structures [13]. The thermal response can be correctly modeled using the equation of three-dimensional heat diffusion, which integrates both of the spatial and temporal distribution of the absorbed laser energy as a heat source term this equation can be written as [14] :

$$\frac{1}{D}\frac{\partial T}{\partial t} = \frac{\partial^2 T}{\partial x^2} + \frac{\partial^2 T}{\partial y^2} + \frac{\partial^2 T}{\partial z^2} + \frac{g(x,y,z)}{k}, \quad (2)$$

where thermal diffusivity can be written as:

$D = \frac{specific\ heat\ capacity \times\ thermal\ conductivity}{density}$, while the absorbed power density can be denotes by $g(x, y, z, t)$ [14].

For a transmission and reflection model in the multilayer structure, as shown in Figure 1.: d is denoted to the thickness of each individual layer while the amplitudes of the incident, amplitudes of the field reflected from the subsequent interface, reflected, and transmitted electromagnetic fields are denote by I, S, R, and T, correspondingly.

The time-averaged power per unit area of a complex electromagnetic wave can be relates to the associated electric and magnetic fields using the Poynting vector (Sm) W/m² which can be expressed as [15]:

$$\langle S_m \rangle = \frac{1}{2}\mathrm{Re}\{E_m \times H_m^*\}. \quad (3)$$

where H_m^* is the magnetic field intensity ($A \cdot m^{-1}$) and E_m is the electrical field.

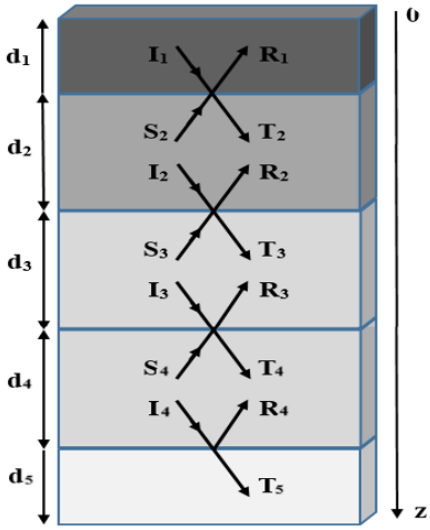

Figure 1: The multilayer concept's transmission reflection system for laser beam.

The power absorbed per unit volume in layer m (Re) can be expressed as:

$$\mathrm{Re}\{-\nabla \cdot \langle S_m \rangle\} = k_0 c \varepsilon_0 n_m \kappa_m |E_m|^2 . \quad (4)$$
$$|E_m|^2 = E_m . \mathrm{E} * .$$

where and k_0 is the wavenumber at the laser wavelength ($k_0 = 2\pi/\lambda$), k and n are the imaginary and real parts of the refractive index.

In each layer the net electric field (E_m) is:

$$E_m = T_m e^{jk_0(n_m + j\kappa_m)z} X + R_m e^{-jk_0(n_m + j\kappa_m)(z-d_m)} X. \quad (5)$$

The electric field's magnitude was determined for all of the layers as follows:

$$|E_m|^2 = |T_m|^2 e^{k_0 \kappa_m^2} + |R_m|^2 e^{k_0 \kappa_m (z-d_m)} + 2|T_m R_m^*| e^{-k_0 \kappa_m d_m} \cos\left(k_0 n_m (2z - d_m) + \varphi_m\right) . \quad (6)$$

In which $\varphi_m = \tan^{-1}\left(\frac{\mathrm{Im}\{T_m R_m^*\}}{\mathrm{Re}\{T_m R_m^*\}}\right)$.

The power density is standardized to the incident power:

$$\mathrm{Re}\left\{-\nabla \cdot \frac{\langle S_m \rangle}{\langle S_i \rangle}\right\}. \quad (7)$$

For the above equations:

- T_m is the complex amplitude of the forward (transmitted) wave in layer m (dimensionless), R_m is the complex amplitude of the backward (reflected) wave in layer m (dimensionless);
- The time-averaged power density of the incident electric field is represented by $\langle \boldsymbol{S}_i \rangle$;
- z represents the position coordinate along the film thickness direction (m) while d_m represents thickness of the m layer;
- k_m represents the imaginary component of the refractive index, while n_i is the refractive indices of the incident and finally n_m denote the transmitted media, thus the normalized power density can be express as:

$$\mathrm{Re}\left\{-\nabla \cdot \frac{\langle \boldsymbol{S}_m \rangle}{\langle \boldsymbol{S}_i \rangle}\right\} = 2k_0 \frac{n_m k_m}{n_i} \frac{|\boldsymbol{E}_m|^2}{I_i^2}. \quad (8)$$

- I_i represents the the incident electric field magnitude, while $\boldsymbol{Em}$ represents the transmitted electric field in layer m and so on. At the initial layer $I_i^2 = \tau_{12}^2 E_1^2$. For the transmission coefficient τ_{12}: $\tau_{12} = 2n_1/(n_1 + n_2)$, where the refractive indices for the FePt layer is n2 and for of air is n1.

3 MATERIALS AND METHODS

The modeled sample comprises a multilayer 3D cubic structure, with the width and depth of each layer clarified in Figure 2.

The ultrafast laser pulses act as the heat source in this investigation, which initiates the thermal excitation within the multilayer structure.

The thermal and optical parameters utilized for determining thermal flow and optical absorption of such properties can be chosen from COMSOL's. This built-in material library provides access to standard from reputable sources [16]. The material properties can be also manually inputted based on empirical data.

Table 1: Simulation parameters which were used in the calculation.

Parameters	Unit	Value
Mesh size	/	fine
Laser wavelength	m	8E-7
Laser spot area	m²	1.131E-8
Peak laser power	W	2.0271E6
Laser power density	W/m²	1.7923E14

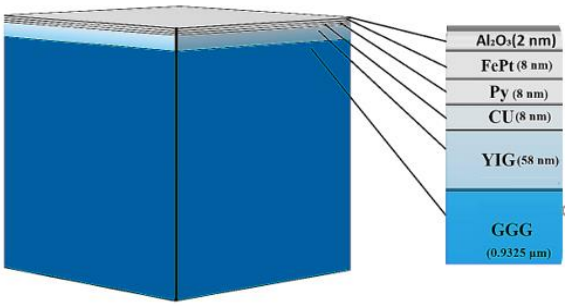

Figure 2: Illustration of the layers and their thicknesses used in this simulation.

Some of the simulation parameters that were used in COMSOL can be seen in Table 1.

The properties of the materials utilized in this study are regarded as temperature-invariant and are presumed to remain constant during the simulation, and can be shown in Table 2.

Thermal boundary layer was included in the calculations and was obtain from previous study [9], [12] and some of it were assumed.

4 RESULTS AND DISCUSSIONS

The distribution of temperature within the tetralayer sample can be observed in Figure 3 where the temperature gradient arises from optical pumping using an ultrafast (fs) pulsed laser with set time delays. This sequence clearly visualizes the transition from highly localized, ultrafast surface heating immediately after the laser pulse hit the very top surface, to diffusive thermal spreading and cooling over the time scales through the multilayer stack.

The temperature profiles along the multilayer structure consisting of Al_2O_3, FePt, Py, Cu, and YIG at different times following femtosecond laser excitation can be seen in Figure 4.

The temperature progress reveals the strong dependence of heat dynamics on both the thermal properties of the materials and the interfacial boundary resistances between the model layers.

At earlier time, the heating stayed largely localized. A sharp and rapid temperature rise is then observed within the FePt layer, due to its strong optical absorption.

As time progresses, the heat in FePt begins to diffuse into the adjacent regions, represented by the Py and Cu layers. Py layer displays a moderate temperature rise, lower than FePt layer but still significant. On the other hand, Cu layer displays a more uniform profile, due to its high thermal conductivity, which enhances heat conduction efficiency.

At the interface of Cu/YIG, the temperature decreases significantly. While the YIG layer itself remained at lower temperatures for extended durations, this represents its insulating behaviour that interferes with the heat flow. The observed differences in temperature evolution can be directly related to the
intrinsic thermal and physical parameters summarized in Table 1. For instance, copper's high thermal conductivity (150 $W \cdot m^{-1} \cdot K^{-1}$) enables rapid lateral heat spreading, resulting in the relatively flat temperature profile.

In contrast, YIG's low thermal conductivity (≈6.63 $W \cdot m^{-1} \cdot K^{-1}$) and high specific heat limit heat transport, maintaining cooler temperatures over longer timescales. The step-like discontinuities observed across the FePt/Py and Py/Cu interfaces arise due to mismatches in both thermal conductivity and interfacial resistance, which hinder smooth heat transfer. Hence, the magnitude of each discontinuity reflects the thermal impedance contrast between neighbouring layers.

Table 2: Properties of the materialsat an ambient temperature of 300K which were used in the calculation.

Material properties	Al_2O_3	FePt	Py	Cu	YIG	GGG
Optical refractive index 800 nm	1.759	2.7+j3.5	2.2+j3.6 [18]	0.2499+j5.033	2.19+j2.48*10^{-6} [17]	1.95
Specific heat ($J.kg^{-1}K^{-1}$)	880	450	430	385	578	400
Mass density (kg/m^3)	3890	15300	8700	8930	5170	7080
Heat conduction coefficients ($W.m^{-1}K^{-1}$)	1 - 4.5 [23]	17 [22]	46.4 [21]	150 [20]	6.63 [19]	7.94 [19]

Moreover, FePt's significant temperature rise is not only due to its strong optical absorption (n = 2.7 + j3.5) but also its relatively high mass density (15300 kg/m³), which increases energy confinement. The interplay between these parameters determines the temporal delay in temperature peaks observed between FePt, Py, and YIG layers.

At later times, the system approaches equilibrium, and temperature gradients gradually smooth out. Within the sample, the FePt layer maintains the highest temperature, making it the dominant heat reservoir. The different between both thermal conductivity and heat capacity leads to the layers step-like discontinuities which can be observed across the interfaces.

Overall, the data reveals a pronounced temperature rise within the FePt layer shortly after excitation followed by decrease in temperature within the Py layer. A minor reduction in temperature in the Cu and YIG layers occurs at 0.05 and 1 ns, resulting in a thermal gradient that signifies the creation of spin current. Because it is thought that the spin current may occurred within this interval time [17].

Figure 5 reveals that the FePt region at the surface demonstrates the most rapid and significant temperature increase, exceeding 250 K in a brief timeframe (~10^{-4} ns). This behavior can be attituded to FePt strong optical absorption and its direct exposure to the laser pulse. The FePt/Py interface also experiences a rapid increase in temperature, though slightly delayed and of lower magnitude compared to the FePt surface. The interface reactions are not well known and need to explore by researchers.

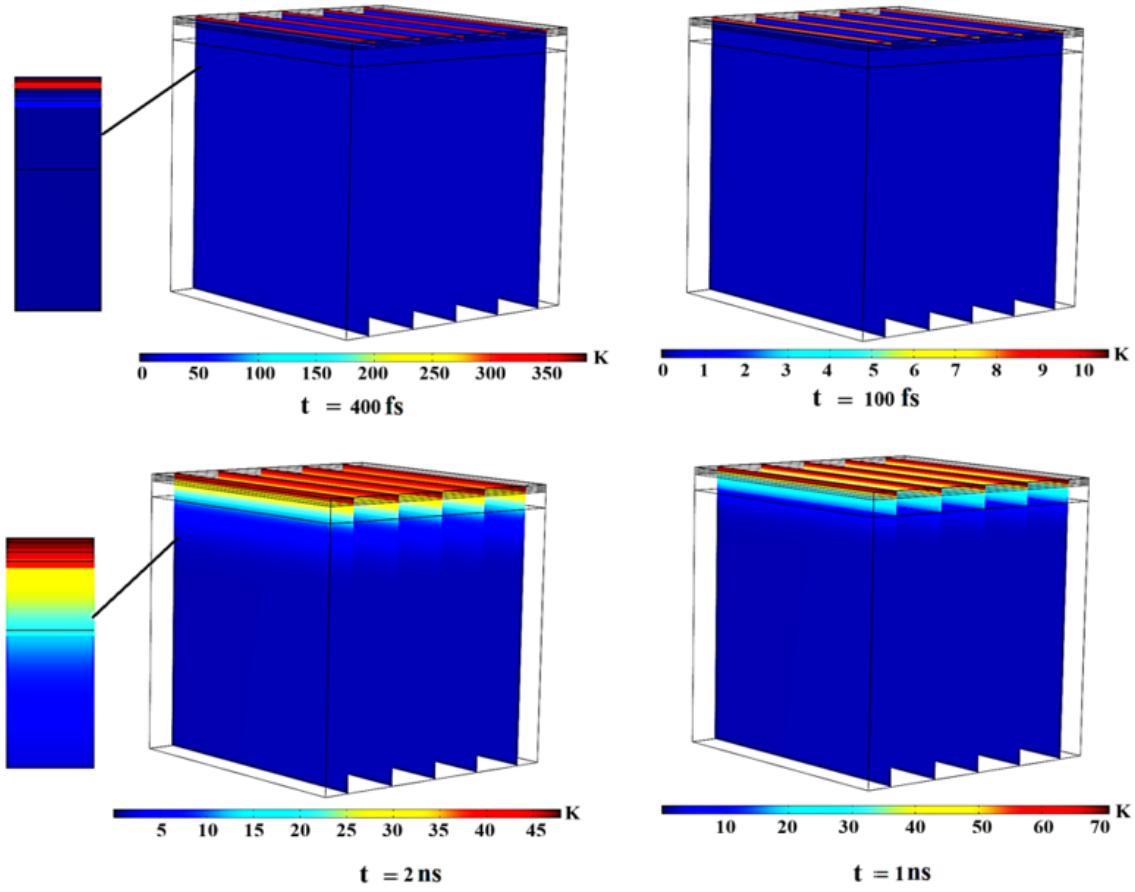

Figure 3: Temperature distribution within the tetralayer specimen at specified time intervals.

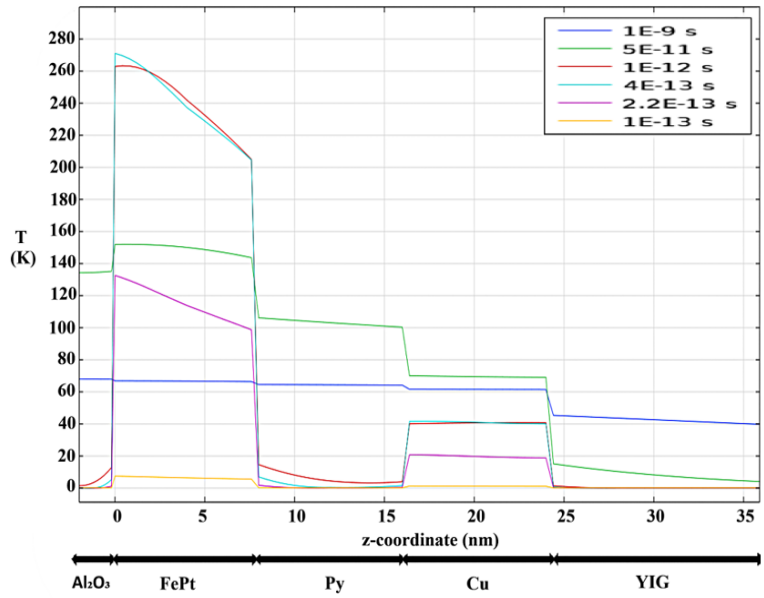

Figure 4: Variation in temperature at specified time intervals.and as a function of depth within the tetralayer sample.

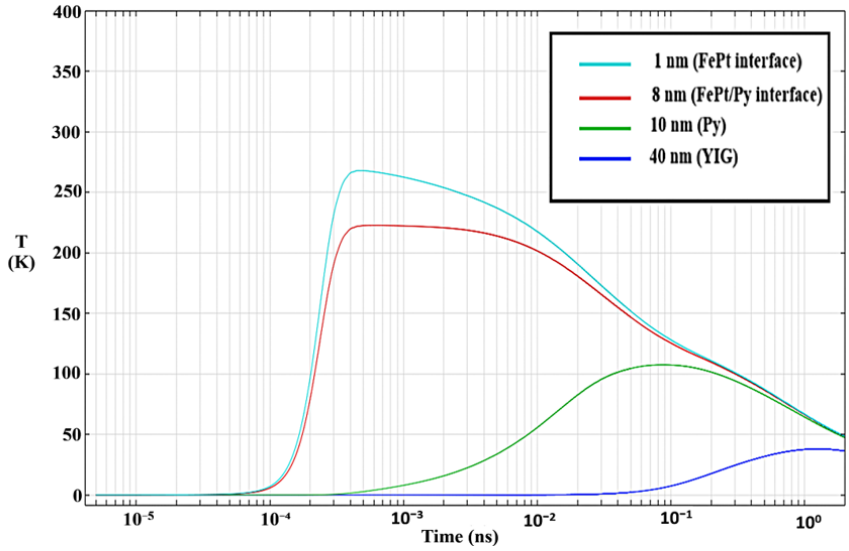

Figure 5: The temperature change in the tetralayer sample as a function of time at specific depths.

As for the Py layer (10 nm) more gradual heating profile were observed, with its peak temperature happening at later times (~$10^{-}3$ ns), because of thermal diffusion from the upper FePt layer. On the other hand, the YIG layer at 40 nm remains rather cool for the initial times, then showing a modest temperature increase. The delayed thermal response is characteristic of buried insulating layers, where heat movement occurs indirectly through interfacial conduction.

Overall, the delay in heating across different depths showed how influential the relationship in the model layers between thermal conductivity, laser absorption, and heat capacity of the material is.

The results emphasize the critical roles of layer positioning and material properties in managing and controlling the ultrafast thermal transport in the tetralayer.

The results were confirmed to have the same behavior as that of the temperature distribution trends and magnitudes reported in previously published data [9], [12].

5 CONCLUSIONS

In this study, COMSOL Multiphysics was used to create a three-dimensional simulation to study the thermal response of a four-layer thin film structure under ultrafast femtosecond laser excitation. Al_2O_3, FePt, Py, Cu, and YIG multilayer films was subjected to optical pumping, and the subsequent heat transfer dynamics were analyzed. Several key insights into the ultrafast thermal behavior of nanoscale heterostructures were noticed:

The simulation results clearly demonstrate that the FePt layer, which is directly exposed to the incident laser pulse, experiences the most rapid and highest temperature rise among all layers. This behavior is attributed to its high optical absorption coefficient, large mass density, and strong electron–phonon coupling.

Within an extremely short time scale on the order of 10^{-4} ns, the temperature in the FePt layer exceeds 250 K above the initial ambient temperature. This thermal response shows the important role of FePt as the primary heat absorber and energy reservoir in the tetralayer system.

Such behavior is very effective in HAMR applications, in which both localized and ultrafast heating is required.

This pronounced thermal response was followed by a delayed yet noticeable increase in the Py and Cu layers, showing the effect of interfacial heat resistance and the different thermal conductivity of the layers.

After this rapid heating of the FePt layer, heat diffusion into the adjacent Py layer is observed with a slight delay and reduced magnitude. This behavor is governed by both the different thermal conductivity between FePt and Py and the presence of interfacial thermal resistance.

The Py layer exhibits a moderate but clearly detectable temperature rise which confirm that Py contributes not only as a magnetic medium but also as a thermal bridge that regulates energy flow between the FePt layer and the deeper layers of the model.

The temperature profile within the Cu layer mostly flat compared to the ferromagnetic layers. This show the critical role of Cu as both a spacer layer and a heat conductor that redistributes thermal energy across the structure.

The presence of the Cu layer is important as it smooth the temperature gradient and at the same time still allowing sufficient thermal flow toward the magnetic insulator.

The YIG layer, being a magnetic insulator, maintained relatively low temperatures for longer durations, confirming its role as a thermal barrier and a stabilizing substrate in spintronic stacks.

Distribution of the temperature data shows noticeable thermal gradient formation across the YIG interface. This thermal gradient is is very important as it indicate the creation of spin current via the spin Seebeck effect, which is especially relevant for spintronic applications.

One of the most significant outcomes of this work is the clear demonstration of thermal gradient formation within the tetralayer structure, the simulation shows that the most effective time for spin current generation happen between approximately 0.05 ns and 1 ns after the laser excitation, where temperature differences between FePt, Py, Cu, and YIG are maximized.

This observation is consistent with previously reported experimental and theoretical studies on ultrafast spin current and validates the physical accuracy of the present model.

Furthermore, the results emphasize the critical dependence of ultrafast thermal transport on material-specific parameters such as thermal conductivity, specific heat capacity, mass density, and optical refractive index in the multilayer system.

This study findings provide a solid theoretical foundation for future experimental investigations and offer practical design guidelines for ultrafast spintronic and HAMR applications.

Future studies may use different materials or further investigate various simulation outcomes by examine different material thicknesses to achieve more enhanced thermal and spin transport properties.

REFERENCES

[1] P. J. Rajput, S. U. Bhandari, and G. Wadhwa, “A Review on-Spintronics an Emerging Technology,” Silicon, vol. 14, no. 15, pp. 9195-9210, 2022/10/01 2022, [Online]. Available: https://doi.org/10.1007/s12633-021-01643-x.

[2] S. M. J. J. o. S. Yakout and N. Magnetism, “Spintronics: Future Technology for New Data Storage and Communication Devices,” vol. 33, pp. 2557-2580, 2020, [Online]. Available: https://doi.org/10.1007/s10948-020-05545-8.

[3] M. Hernandez et al., “Laser thermal processing for ultra shallow junction formation: numerical simulation and comparison with experiments,” Applied Surface Science, vol. 208, pp. 345-351, 2003, [Online]. Available: https://doi.org/10.1016/S0169-4332(02)01395-8.

[4] S. Niu et al., "Recent Advances in Applications of Ultrafast Lasers," Photonics, vol. 11, no. 9, p. 857, 2024, [Online]. Available: https://www.mdpi.com/2304-6732/11/9/857.

[5] K. Sugioka and Y. Cheng, "Ultrafast lasers-reliable tools for advanced materials processing," Light: Science & Applications, vol. 3, no. 4, pp. e149-e149, 2014, [Online]. Available: https://doi.org/10.1038/lsa.2014.30.

[6] W.-H. Hsu and R. H. Victora, "Heat-assisted magnetic recording - Micromagnetic modeling of recording media and areal density: A review," Journal of Magnetism and Magnetic Materials, vol. 563, p. 169973, 2022/12/01 2022, [Online]. Available: https://doi.org/10.1016/j.jmmm.2022.169973.

[7] S. Isogami et al., "Thermal spin-torque heat-assisted magnetic recording," Acta Materialia, vol. 286, p. 120743, 2025, [Online]. Available: https://doi.org/10.1016/j.actamat.2025.120743.

[8] G. Ju et al., "High density heat-assisted magnetic recording media and advanced characterization-Progress and challenges," IEEE Transactions on Magnetics, vol. 51, no. 11, pp. 1-9, 2015, [Online]. Available: https://doi.org/10.1109/INTMAG.2015.7156491.

[9] M. A. Abdul-Hussain and H. J. Mohamad, "Thermal Effect in a 3-D Simulation within Multilayer Thin Film of Ultrafast-Pulsed Laser," Al-Mustansiriyah Journal of Science, vol. 32, no. 4, pp. 104-109, 2021, [Online]. Available: http://doi.org/10.23851/mjs.v32i4.1039.

[10] U. Keller and R. Paschotta, Ultrafast lasers. Springer, 2021, [Online]. Available: https://doi.org/10.1007/978-3-030-82532-4.

[11] J. Kimling and D. G. Cahill, "Spin diffusion induced by pulsed-laser heating and the role of spin heat accumulation," Physical Review B, vol. 95, no. 1, p. 014402, 2017, [Online]. Available: https://doi.org/10.1103/PhysRevB.95.014402.

[12] H. J. Mohamad and B. H. Hamza, "Thermal Simulation for Ultrafast Laser in Multilayered Sample for Heat-Assisted Magnetic Recording Application," Baghdad Science Journal, vol. 22, no. 6, pp. 1930-1939, 2025, [Online]. Available: https://doi.org/10.21123/2411-7986.4967.

[13] G. Neuber et al., "Temperature-dependent spectral generalized magneto-optical ellipsometry," Applied Physics Letters, vol. 83, no. 22, pp. 4509-4511, 2003, [Online]. Available: https://doi.org/10.1063/1.1629145.

[14] A. M. Hofmeister, "Thermal diffusivity of garnets at high temperature," Physics and Chemistry of Minerals, vol. 33, no. 1, pp. 45-62, 2006, [Online]. Available: https://doi.org/10.1007/s00269-005-0056-8.

[15] W. Liu, Y. Yang, and M. Asheghi, "Thermal and electrical characterization and modeling of thin copper layers," in Thermal and Thermomechanical Proceedings 10th Intersociety Conference on Phenomena in Electronics Systems, 2006. ITHERM 2006., 2006: IEEE, pp. 1171-1176, [Online]. Available: https://doi.org/10.1109/ITHERM.2006.1645477.

[16] J. Hurst, P.-A. Hervieux, and G. Manfredi, "Spin current generation by ultrafast laser pulses in ferromagnetic nickel films," Physical Review B, vol. 97, no. 1, p. 014424, 2018, [Online]. Available: https://doi.org/10.1103/PhysRevB.97.014424.

[17] E. Mirkoohi, D. E. Seivers, H. Garmestani, and S. Y. Liang, "Heat source modeling in selective laser melting," Materials, vol. 12, no. 13, p. 2052, 2019, [Online]. Available: https://doi.org/10.3390/ma12132052.

[18] A. Crook, "The reflection and transmission of light by any system of parallel isotropic films," Journal of the Optical Society of America, vol. 38, no. 11, pp. 954-964, 1948, [Online]. Available: https://doi.org/10.1364/JOSA.38.000954.

[19] C. Multiphysics, "Comsol multiphysics reference manual," COMSOL: Grenoble, France, vol. 1084, p. 834, 2023.

[20] T. Goto, M. C. Onbaşlı, and C. Ross, "Magneto-optical properties of cerium substituted yttrium iron garnet films with reduced thermal budget for monolithic photonic integrated circuits," Optics Express, vol. 20, no. 27, pp. 28507-28517, 2012, [Online]. Available: https://doi.org/10.1364/OE.20.028507.

[21] B. Su-Yuan, T. Zhen-An, H. Zheng-Xing, Y. Jun, and W. Jia-Qi, "Thermal conductivity measurement of submicron-thick aluminium oxide thin films by a transient thermo-reflectance technique," Chinese Physics Letters, vol. 25, no. 2, p. 593, 2008, [Online]. Available: https://doi.org/10.1088/0256-307X/25/2/065.

[22] A. Giri, S. H. Wee, S. Jain, O. Hellwig, and P. E. Hopkins, "Influence of chemical ordering on the thermal conductivity and electronic relaxation in FePt thin films in heat assisted magnetic recording applications," Scientific Reports, vol. 6, no. 1, p. 32077, 2016, [Online]. Available: https://doi.org/10.1038/srep32077.

[23] Avery, S. Mason, D. Bassett, D. Wesenberg, and B. Zink, "Thermal and electrical conductivity of approximately 100-nm permalloy, Ni, Co, Al, and Cu films and examination of the Wiedemann-Franz Law," Physical Review B, vol. 92, no. 21, p. 214410, 2015, [Online]. Available: https://doi.org/10.1103/PhysRevB.92.214410.